

Isospin Splitting of the Giant Dipole Resonance in $^{60}\text{Ni}^\dagger$

E. M. Diener, J. F. Amann, and P. Paul*

Department of Physics, State University of New York, Stony Brook, New York 11790

and

S. L. Blatt

State University of New York, Stony Brook, New York 11790

and The Ohio State University, Columbus, Ohio 43210 ‡

(Received 25 November 1970)

The radiative-capture reaction $^{59}\text{Co}(p, \gamma)^{60}\text{Ni}$ has been studied for proton energies from 4.40 to 13.60 MeV. Cross-section and angular-distribution data were measured with a large anticoincidence-shielded NaI(Tl) detector. The yield curve for ground-state capture shows two broad peaks, at ^{60}Ni excitations of 16.6 and 19.6 MeV; these are interpreted as the $T_<$ and $T_>$ components of the giant dipole resonance. The results of a detailed calculation ignoring isospin effects do not adequately explain all of the observations; a simple 1p-1h calculation using eigenfunctions of T describes the results quite well. The first-excited-state-capture yield curve is similar to the ground-state curve, shifted in energy by ~ 300 keV. The data suggest that most of the observed strength in the giant dipole resonance based on the first excited state of ^{60}Ni is concentrated in 2^- states.

I. INTRODUCTION

The topic of isospin effects observable in the giant-dipole-resonance (GDR) region of nuclei has been of interest for almost two decades,¹⁻⁴ but only in the last few years have detailed calculations been performed⁵⁻⁸ and compared with experiments designed to observe these effects. For a nucleus with $N \neq Z$ and ground-state isospin $T_0 = |T_z|$, one effect predicted is that the GDR will exhibit two isospin components. The component at lower energy will be characterized by $T = T_0 \equiv T_<$, while the component at higher energy will have $T = T_0 + 1 \equiv T_>$. Writing the giant-dipole state as $\psi_D = C_<\phi_< + C_>\phi_>$, the relative intensities of the two isospin components are given, according to Goulard and Fallieros,⁶ as

$$|C_<|^2 = \frac{T_0}{T_0 + 1} \left[\frac{1 + 1.5/A^{2/3} - 4T_0(T_0 + 1)/A^2}{1 - 4(T_0/A)^2} \right] \quad (1a)$$

and

$$|C_>|^2 = \frac{1}{T_0 + 1} \left[\frac{1 - 1.5(T_0/A^{2/3})}{1 - 4(T_0/A)^2} \right]. \quad (1b)$$

The first factor of the right-hand side is the square of an isospin Clebsch-Gordan coefficient, while the expression inside the brackets corrects for the fact that fewer configurations contribute to the $T_>$ component than to the $T_<$ component. We observe that $|C_>|^2$ decreases rapidly as A and T_0 increase, as is shown in Table I.

The energy separation of the two components is given approximately by⁹

$$\Delta E = E_{T_>} - E_{T_<} = \tilde{U}(T_0 + 1)/T_0, \quad (2a)$$

where \tilde{U} is the symmetry energy U from the Lane potential reduced by a factor which takes into account that the coherent $T_<$ giant-dipole state is pushed up more in energy than is the coherent $T_>$ giant-dipole state. This again is because a larger number of configurations contributes to the $T_<$ state.⁷ Taking the symmetry energy $U = 100T_0/A$ (MeV), an approximate expression for \tilde{U} is $\tilde{U} \cong 60T_0/A$ (MeV), and hence

$$\Delta E = 60(T_0 + 1)/A \text{ (MeV)}. \quad (2b)$$

The factor of 60 appearing in the equation for \tilde{U} has been derived by Fallieros⁹ and yields values of ΔE in good agreement with other experimental evidence for isospin splitting for the GDR.¹⁰⁻¹² The last column of Table I gives some predicted values of ΔE .

On the assumption of isospin conservation, neutron decay of the $T_> = T_0 + 1$ GDR to low-lying states in the $T_z = T_0 - \frac{1}{2}$ nucleus is generally prohibited, since these states normally have $T = T_z$. Proton decay, however, is allowed to all levels of the $T_z = T_0 + \frac{1}{2}$ residual nucleus and, in general, should be the dominant decay channel of the $T_>$ GDR. The (p, γ) and (γ, p) reactions are therefore favorable reactions for investigation of the $T_>$ GDR.

Radiative-proton-capture experiments which have been interpreted in terms of isospin splitting of the GDR have been performed at Argonne National Laboratory [$^{37}\text{Cl}(p, \gamma_0)^{38}\text{Ar}$],¹³ Stanford [$^{87}\text{Rb}(p, \gamma_0)^{88}\text{Sr}$ and $^{89}\text{Y}(p, \gamma_0)^{90}\text{Zr}$],¹⁰ and Stony Brook [$^{88}\text{Sr}(p, \gamma_0)^{89}\text{Y}$, $^{88}\text{Sr}(p, \gamma_1)^{89}\text{Y}$],¹¹ and [$^{41}\text{K}(p, \gamma_0)^{42}\text{Ca}$].¹² The experiments in the mass-90 region coupled with calculations for ^{88}Sr ,⁷ ^{89}Y ,¹⁴ and ^{90}Zr ⁸ seem to give clear evidence for discrete $T_>$

giant-dipole states ~ 4 – 5 MeV above the broad $T_{<}$ GDR.

Photonuclear reaction measurements in the GDR region of $T_z \neq 0$ nuclei have been mostly by the (γ, n) reaction. In several cases where proton decay has also been observed,^{15–20} the peak in the proton yield occurs at a higher γ -ray energy than the peak in the neutron yield, indicating the possibility of isospin splitting of the GDR.^{2, 3} In general, however, the lack of data for the proton channel makes it difficult to interpret weak peaks which are observed in the (γ, n) reaction above the main $T_{<}$ GDR in terms of $T_{>}$ dipole states. This is because they may also be attributed to the giant quadrupole resonance (GQR) (e.g., a recent case in the tin isotopes²¹) or may be the result of coupling between the $T_{<}$ GDR and surface oscillations.²²

The present work is an investigation of isospin effects in the GDR in ^{60}Ni observed through radiative proton capture. As can be seen from Table I, the nucleus ^{60}Ni , with four excess neutrons, is a desirable case in which to investigate isospin effects in the GDR. The $^{60}\text{Ni}(\gamma, n)$ reaction has been measured by several groups,^{23–25} albeit with somewhat conflicting results. Although all (γ, n) data indicate that the main $T_{<}$ dipole strength is distributed over several MeV, the expected 3-MeV separation between $T_{>}$ and $T_{<}$ components should be sufficient to resolve them. In addition, on the basis of Eq. 1, the $T_{>}$ component is expected to contain $\sim 30\%$ of the dipole strength and should be observable as a strong peak in the $^{59}\text{Co}(p, \gamma_0)$ reaction at an excitation energy where essentially no enhancement of the $^{60}\text{Ni}(\gamma, n)$ yield occurs. Based on total absorption and (γ, n) data, Min²⁶ has interpreted the photodisintegration of ^{60}Ni in the GDR region in terms of isospin splitting with the $T_{<}$ and $T_{>}$ components at 17 and 22.5 MeV, respectively. The data for the $^{59}\text{Co}(p, \gamma_0)$ reaction reported here, used in conjunction with the $^{60}\text{Ni}(\gamma, n)$ data,²³ indicate that the $T_{<}$ and $T_{>}$ components of the GDR occur at 16.6 and 19.6 MeV, respectively, and that the strength observed above 21 MeV is perhaps related to the GQR.

TABLE I. Predictions of effects due to isospin splitting of the GDR. $|C_{>}|^2$ is the relative intensity of the $T_{>}$ component and ΔE the energy separation between $T_{>}$ and $T_{<}$ components.

Nucleus	T_0	$ C_{>} ^2$	ΔE (MeV)
^{42}Ca	1	0.44	2.86
^{60}Ni	2	0.27	3.00
^{66}Zn	3	0.18	3.64
^{90}Zr	5	0.11	4.00

II. EXPERIMENTAL PROCEDURE AND DATA ANALYSIS

Cross sections and angular distributions of the ground and 1.33-MeV first-excited-state-capture γ rays (referred to below as γ_0 and γ_1 , respectively) were measured for the reaction $^{59}\text{Co}(p, \gamma)^{60}\text{Ni}$ over the bombarding energy range 4.40 to 13.60 MeV. The reaction has a Q value of 9.527 MeV, hence the γ rays of interest had energies ranging from 12.6 to 23.1 MeV. The procedures used in these measurements are described immediately below; data analysis methods are given in the second part of this section.

The proton beam was obtained from the State University of New York at Stony Brook tandem Van de Graaff accelerator. Data were taken at 100-keV intervals from 6.40 to 11.40 MeV, and at 200-keV intervals from 4.40 to 6.40 MeV and from 11.40 to 13.60 MeV. Beam current at the target varied from 200 nA at 4.40 MeV to 50 nA at 13.60 MeV and was adjusted so that the counting rate in the γ -ray detection system remained below predetermined limits, as described below. Running time per data point at bombarding energies above 10 MeV was approximately 1 h.

Targets were prepared by evaporating metallic cobalt (100% ^{59}Co) on to 50- $\mu\text{g}/\text{cm}^2$ carbon foils. Target thickness was determined by measuring the energy loss of 5.486-MeV α particles from an ^{241}Am source in passing through the target. After correcting for the energy loss in the carbon foil, the target thickness was found to be 1.2 mg/cm^2 , or 35-keV to 10-MeV protons.

The γ -ray detector consisted of a 25-cm \times 25-cm NaI crystal surrounded by a plastic anticoincidence shield and has been described in detail elsewhere.²⁷ For the measurement of γ -ray yield as a function of proton energy, the detector was positioned at 90° with respect to the beam with the front face of the crystal 30 cm from the target. The solid angle of 0.113 sr subtended by the detector was defined by a lead collimator projecting onto the full back face of the NaI crystal. For angular distribution measurements the detector was moved back 20 cm so that it could be moved azimuthally from 35 to 145° with respect to the beam direction. The crystal, shield, and associated electronics were designed to give good resolution at high counting rates, e.g., for a 20-MeV γ ray, and a total NaI counting rate of 10^5 counts/sec, 4.5% resolution was obtained. In this experiment, the counting rate in the NaI remained below 2×10^5 counts/sec. In order to maintain a low rate of random rejections of NaI signals by the shield, the beam current was limited so that the counting rate in the shield did not exceed 10^6 counts/sec. With

the fast anticoincidence logic used, this gave an estimated random rejection rate of $<4\%$ of the NaI counting rate.

Figure 1 shows a γ -ray pulse-height spectrum obtained at a bombarding energy of 7.60 MeV. Using standard line shapes and a least-squares computer fitting procedure, simultaneous fits to the γ_0 , γ_1 , and background peaks were made as described below. Line shapes for various γ energies were obtained from the $T(p, \gamma)^4\text{He}$, $^{39}\text{K}(p, \gamma)^{40}\text{Ca}$, and $^{12}\text{C}(p, \gamma)^{13}\text{N}$ reactions. The resolution improves slowly with increasing γ energy but deteriorates with increasing over-all counting rate. Since the total counting rate increased monotonically with bombarding energy, it turned out to be feasible to use one standard line shape throughout the energy region covered in this experiment. The same line shape was used to fit both the γ_0 and γ_1 peaks which differ in energy by only 1.33 MeV. In general, the background in the region of γ_0 and γ_1 was obtained from the high-energy side of a standard line shape, fitted to the sharp rise in the pulse-height spectrum which occurs below the γ_1 peak. This procedure yields good fits with normalized χ^2 values between 0.5 and 1.5. The dashed lines of Fig. 1 indicate the fits to γ_0 and γ_1 obtained in the above manner.

Since the target is on a carbon backing, γ radiation from proton reactions on carbon must be considered as background contributions in the experimental spectra. The highest-energy γ ray from protons on carbon comes from the reaction $^{13}\text{C}(p, \gamma)^{14}\text{N}$. This reaction has a Q value of 7.55 MeV, placing the contaminant γ ray below both γ_0 and γ_1 from the reaction under study at all bombarding energies. At the lowest energy considered in this reaction, the separation of the γ rays from the $^{13}\text{C}(p, \gamma)$ and the $^{59}\text{Co}(p, \gamma)$ reactions is 0.89 MeV. As the bombarding energy increases, the center-of-mass correction increases the separation. In Fig. 1 the highest energy at which γ rays from radiative capture on ^{13}C can occur is indicated. As can be seen, even for γ_1 the $^{13}\text{C}(p, \gamma)$ reaction poses no problem.

Absolute cross sections were obtained from the γ yield by direct calculation, which requires knowledge of target thickness, total charge which entered the target, the solid angle subtended by the detector, and the efficiency of the detector. The latter consists of the intrinsic efficiency of the collimated NaI crystal which was taken as 100% (after correction for absorption in materials between the target and crystal) and the electronics rejection ratio. This latter could be obtained for each run from the accepted and rejected spectra, stored separately in a pulse-height analyzer. The calculation yielded the number 0.029 sr for the

product of solid angle and efficiency. A check on this calculation was made by a comparison with the known absolute thick-target yield from the $^{12}\text{C}(p, \gamma)^{13}\text{N}$ reaction from the first $T = \frac{3}{2}$ resonance²⁸ at $E_p = 14.231$ MeV, and agreement was within 3%.

III. RESULTS

A. Ground-State Transition

Figure 2 displays the data obtained at 90° for the excitation function of the ground-state transition. The solid line through the data points is intended merely to guide the eye. The uncertainty associated with the data points is $\pm 10\%$ of the yield, based on counting statistics and computer line-fitting accuracy, while a total uncertainty of $\pm 30\%$ is assigned to the absolute cross section due to

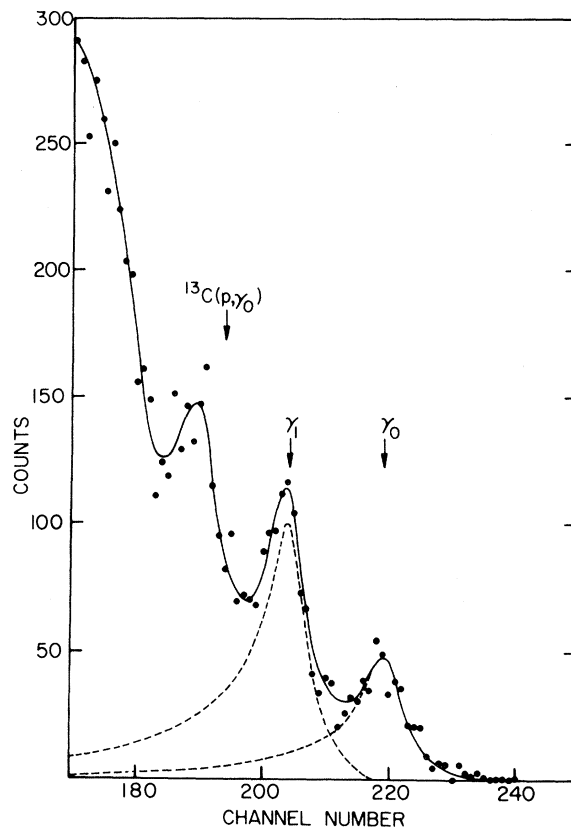


FIG. 1. Spectrum of high-energy γ rays from radiative capture of protons by ^{59}Co . Only the region of the pulse-height spectrum which corresponds to $E_\gamma > 13$ MeV is shown. The 7.6-MeV bombarding energy results in 17.00- and 15.67-MeV γ rays from the ground-state (γ_0) and first-excited-state (γ_1) transitions, respectively. The next lower peak is due to transitions to a group of higher excited states in ^{60}Ni . Also indicated is the position at which γ rays from the reaction $^{13}\text{C}(p, \gamma)^{14}\text{N}$ would appear. The dashed lines indicate the contributions from the γ_0 and γ_1 transitions obtained by fitting the data as described in the text.

additional uncertainties in the target thickness and detector efficiency determinations. The reproducibility of the data was checked at 25% of the data points and agreement obtained within the 10% standard deviation in yield. Since the target thickness is less than the energy separation between the data points, fine structure of a width less than 100 keV may have been missed. We note that the fluctuating structure observed in Fig. 2 is typical of (p, γ) excitation functions in the giant-resonance region of other medium-weight nuclei.^{12, 13, 29} Another point of interest is that the maximum cross section of $0.89 \mu\text{b/sr}$ at $E_p = 10.0$ MeV is quite small, e.g., for the purpose of comparison it is only $\sim 12\%$ of the maximum value observed²⁹ in $^{39}\text{K}-(p, \gamma_0)^{40}\text{Ca}$ at 90° .

Averaging the data of Fig. 2 over a 600-keV energy interval and using detailed balance to obtain the cross section of the inverse reaction $^{60}\text{Ni}(\gamma, p_0)$ gives the excitation function shown by the data points in Fig. 3. The data indicate the existence of four peaks in the energy region 15 to 23 MeV. A fitting procedure using resonance shapes³⁰

$$\sigma(E) = \frac{\sigma_0}{1 + (E^2 - E_0^2)^2 / (\Gamma E)^2} \quad (3)$$

gives peak positions at 16.6, 19.6, 21.7, and 22.7 MeV with relative heights of 1.0, 1.5, 0.2, and 0.8, respectively. It is evident from Fig. 3 that the shapes of the $^{60}\text{Ni}(\gamma, n)$ and $^{60}\text{Ni}(\gamma, p_0)$ yields differ dramatically in the region of excitation between 15 and 21 MeV. Whereas a peak occurs at 16.6 MeV relatively weakly in the (γ, p_0) reaction a peak at 17.0 MeV dominates the (γ, n) reaction. Conversely, a 19.6-MeV peak appears relatively strongly in (γ, p_0) but very weakly in (γ, n) . This is in agreement with the behavior expected of the T_- and T_+ components of the GDR. Although the

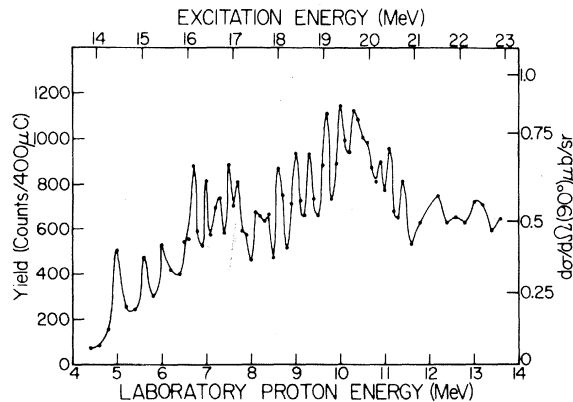


FIG. 2. Excitation function for the reaction $^{59}\text{C}(p, \gamma_0)^{60}\text{Ni}$. The solid line is intended merely to guide the eye. The uncertainty associated with each data point is $\pm 10\%$ of the yield.

data of Goryachev *et al.*²⁴ and of Owen, Muirhead, and Spicer²⁵ conflict with that of Min and White,²³ both show the major dipole strength in the 17- to 18-MeV region with either decreasing cross section or a local minimum at 19.6 MeV. Hence, neither is in conflict with the observation that a state at 19.6 MeV appears strongly only in the proton channel. In the following discussion we subjectively select the results of Min and White²³ for purposes of comparison.

Angular distributions measured in the GDR region have been fitted with a sum of Legendre polynomials, $W(\theta) = 1 + A_1 P_1(\cos\theta) + A_2 P_2(\cos\theta)$. The results are listed in Table II. In general, large negative values of A_2 have been observed for many nuclei in the GDR. This is because the major contribution to the dipole strength generally comes from transitions between orbits with l_j equal to $(l+1)_{i+1+\frac{1}{2}}$ and $(l)_{i+\frac{1}{2}}$. For example, the dominant one-particle-one-hole component in the wave function of the ^{60}Ni giant-dipole state is expected to be the $g_{9/2}(f_{7/2})^{-1}$ configuration. For the reaction $^{59}\text{Co}-(p, \gamma_0)^{60}\text{Ni}$, the $E1$ transition between $g_{9/2}$ and $f_{7/2}$ orbits is characterized by $A_2 = -0.33$. However, the values we observe for A_2 are positive. One possible explanation for this is that the GDR is essentially a $g_{7/2}f_{7/2}^{-1}$ excitation. Alternatively, interference between various 1p-1h configurations of the giant-dipole state can lead to positive values of A_2 . Both explanations will be discussed below. We note also that the positive value observed for A_1 at $E_p = 10.0$ MeV is indicative of interference be-

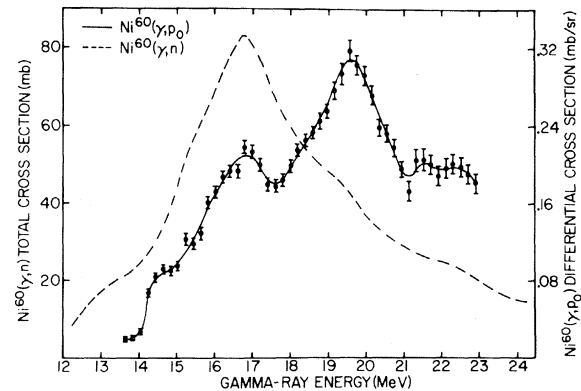


FIG. 3. Excitation functions for the reactions $^{59}\text{Ni}-(\gamma, p_0)^{59}\text{C}$ at 90° , obtained by detailed balance from the data of Fig. 1 averaged over a 600-keV interval, and $^{60}\text{Ni}(\gamma, n)^{60}\text{Ni}$ obtained from Ref. 23. Note the different cross-section scales for the two reactions. Above the $^{60}\text{Ni}(\gamma, 2n)$ threshold, the photoneutron data have been corrected for multiple neutron emission to yield the $^{60}\text{Ni}(\gamma, n)$ cross section. The indicated error bars were obtained from the averaging procedure. The solid line through the $^{60}\text{Ni}(\gamma, p_0)$ data points is drawn to guide the eye.

TABLE II. Coefficients obtained by fitting a sum of Legendre polynomials $W(\theta) = 1 + \sum A_i P_i(\cos\theta)$, $i = 1, 2$, to the $^{59}\text{Co}(p, \gamma_0)^{60}\text{Ni}$ angular distributions at various excitation energies E_x in ^{60}Ni . The goodness of the fit is indicated by the normalized χ^2 value listed in the last column.

E_p (MeV)	E_x (MeV)	A_1	A_2	χ^2
6.70	16.12	$+0.02 \pm 0.03$	$+0.03 \pm 0.05$	1.5
7.55	16.95	$+0.08 \pm 0.05$	$+0.16 \pm 0.07$	1.5
7.60	17.00	-0.01 ± 0.02	$+0.28 \pm 0.03$	0.6
10.00	19.36	$+0.22 \pm 0.03$	$+0.07 \pm 0.04$	1.5

tween $E1$ and $M1$ or $E2$ radiation.

Assuming a smoothly varying value of A_2 throughout the energy region studied in this experiment, the data imply an integrated cross section of 24.5 MeV mb for the (γ, p_0) reaction, or 2.5% of the classical dipole sum rule. This is quite small in comparison to the integrated cross section of the $^{60}\text{Ni}(\gamma, n)$ reaction which, up to 25 MeV, exhausts 60% of the classical dipole sum rule.²³

B. First-Excited-State Transition

The excitation function for the transition to the $J^\pi = 2^+$ first excited state of ^{60}Ni is shown in Fig. 4. It shows fine and gross structure similar to that observed in the γ_0 excitation function. The gross structure is brought out more clearly in Fig. 5, where the data have been averaged over a 600-keV interval. This smoothed excitation function exhibits five peaks, at 14.7, 17.2, 19.6, 20.6, and 22.5 MeV. In general, the excitation function for the excited state is expected to show more complexity than the γ_0 curve since $E1$ transitions are allowed from 1^- , 2^- , and 3^- states. However, the averaged curves for γ_1 and γ_0 exhibit a strong cor-

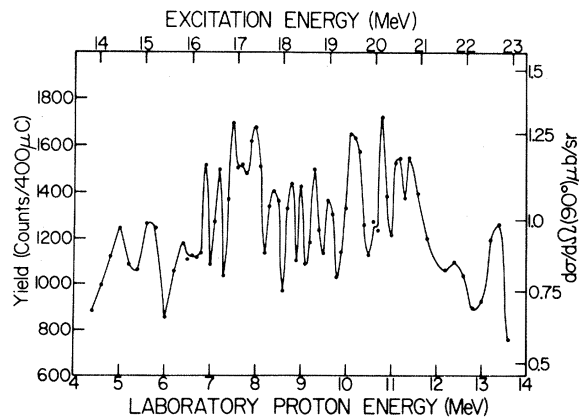


FIG. 4. Excitation curve for the reaction $^{59}\text{Co}(p, \gamma_1)^{60}\text{Ni}$. The zero on the ordinate has been suppressed. The solid line drawn through the data merely connects the points.

TABLE III. Coefficients obtained by fitting a sum of Legendre polynomials $W(\theta) = 1 + \sum A_i P_i(\cos\theta)$, $i = 1, 2$, to the $^{59}\text{Co}(p, \gamma_1)^{60}\text{Ni}$ angular distributions at various excitation energies E_x in ^{60}Ni . The goodness of the fit is indicated by the normalized χ^2 values listed in the last column.

E_p (MeV)	E_x (MeV)	A_1	A_2	χ^2
6.70	16.12	$+0.07 \pm 0.02$	$+0.02 \pm 0.03$	0.6
7.60	17.00	$+0.13 \pm 0.07$	-0.27 ± 0.10	0.7
10.00	19.36	$+0.02 \pm 0.03$	-0.23 ± 0.05	1.0

relation of the peak positions if the γ_1 curve is shifted down in energy by 300 keV with respect to the γ_0 curve. This observation will be further discussed below.

Angular distribution coefficients are listed in Table III. The small values observed for A_1 indicate little interference. The negative values observed for A_2 at excitation energies greater than 17 MeV are in contrast to the positive values of A_2 found for the γ_0 transition. Assuming a smoothly varying value of A_2 throughout the energy region covered in this experiment, the integrated cross section for the inverse reaction, (γ, p_0) on the first excited state of ^{60}Ni , is 8.84 MeV mb. This is approximately $\frac{1}{3}$ the value given above for the (γ, p_0) reaction on the ground state of ^{60}Ni .

IV. DISCUSSION OF THE GROUND-STATE TRANSITION

The experimental results presented here relate to two separate aspects of the GDR. First, and the central point of this study, is the effect of isospin on the GDR, i.e., the splitting into the $T_>$ and the $T_<$ parts. Although the theoretical approach

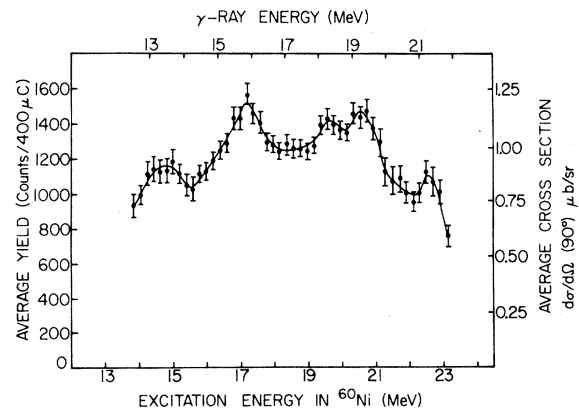


FIG. 5. Averaged excitation function for the reaction $^{59}\text{Co}(p, \gamma_1)^{60}\text{Ni}$ in which the data of Fig. 4 have been averaged over a 600-keV energy interval. The indicated error bars were obtained from the averaging procedure. The solid line through the averaged data is merely to guide the eye.

for calculating this effect has been worked out by Goulard, Hughes, and Fallieros,⁷ detailed calculations are not yet available for ^{60}Ni . However, some rules based on an "averaged" description of the GDR, which are given in the Introduction, predict the energy separation and relative dipole strength of the two parts. The second aspect concerns the general properties of the GDR, exclusive of isospin. [It is seen from the isospin-coupling coefficients of Eq. (1) that the "conventional" GDR of heavy nuclei, such as that observed in the (γ, n) reaction, is to be identified with the T_z part.] In this realm, the properties to be explained in the case of ^{60}Ni , apart from the energy spectrum of the dipole strength, are the almost isotropic angular distribution and the very small proton-capture cross section. A detailed calculation without incorporation of isospin has been done for ^{60}Ni by Ligensa and Greiner³¹ (henceforth referred to as LG). In the following discussion comparison is first made between their predictions and our results. As it turns out, the calculation, although in good agreement with the data at the lower GDR peak, fails to account for the properties of the upper large peak. We then introduce a simple calculation, using wave functions of good isospin, by which the essential features of the data are explained in terms of two isospin components of the GDR. Further evidence supporting this explanation concludes the discussion.

A. Comparison with the Calculation of Ligensa and Greiner

The model used by LG builds up the GDR from $1p$ - $1h$ states coupled to quadrupole surface vibrations, thus spreading the dipole strength over several states. These states are then coupled to the continuum through a residual interaction. This

procedure yields particle as well as γ widths, which makes comparison with the experimental capture cross section straightforward. The total width of each state is larger than the sum of all partial widths calculated in this manner because of the additional spreading width. (It has been shown by Danos and Greiner³⁰ how, in principle, the correct total width can be obtained.) The ground state of ^{60}Ni is taken as doubly closed. The assumption is certainly not very good for the neutron side, as evidenced by the $\frac{3}{2}^-$ spin of ^{61}Ni and the spectroscopic factor of 0.40 obtained by Cohen, Fullmer, and McCarthy³² in the $^{60}\text{Ni}(d, p)^{61}\text{Ni}$ reaction. There is also some evidence³³ that the $f_{7/2}$ shell on the proton side is broken by about 20%. Since experimental numbers for the various single-particle energies are incomplete and, in particular, the $g_{7/2}$ orbital has not yet been located, LG calculate the energies in an average Woods-Saxon potential. Some of the known single-particle energies³²⁻³⁴ are, however, several MeV lower than values obtained by this procedure.

Table IV summarizes the results of LG pertinent to our data. The total cross sections listed in the last column were obtained by using the assumption that ^{59}Co is a pure $f_{7/2}$ hole in a ^{60}Ni core. The total width Γ_{tot} was set equal to the sum of all escape widths Γ . Comparison of the predictions with the averaged cross-section curve of Fig. 3 shows that the main predicted peaks at 16.4, 18.2, and 19.7 MeV can all be associated with peaks or shoulders in the experimental curve. The unpredicted strength which we observe at about 21-MeV excitation energy may be associated with a GQR (such as has been indicated, for instance, by Urbas and Greiner²¹ in the tin isotopes). As has been demonstrated in one example, where the GQR has actually been located experimentally,³⁵ the GQR makes itself felt essentially only

TABLE IV. Parameters of GDR states in ^{60}Ni obtained from the calculation by LG (appropriate dimensions were assigned to all widths). Only proton partial widths for configurations with an $f_{7/2}$ hole are shown, since only these enter into the calculation of the $^{59}\text{Co}(p, \gamma_0)$ cross sections, as described in the text. The results are given in the last column.

$E(\text{MeV})$	Configuration	$\Gamma_p(l, j)$ (MeV)	$\Gamma(\text{MeV})$	$\Gamma_\gamma(\text{eV})$	$\sigma(p, \gamma_0)$ (μb)
16.35	$g_{7/2}(f_{7/2})^{-1}$	0.3	0.43	428	7.91
	$g_{9/2}(f_{7/2})^{-1}$	0.2			
18.18	$g_{7/2}(f_{7/2})^{-1}$	0.03	0.06	185	2.23
	$g_{9/2}(f_{7/2})^{-1}$	0.05			
19.17	$g_{7/2}(f_{7/2})^{-1}$	0.00	0.55	21	0.03
	$g_{9/2}(f_{7/2})^{-1}$	0.01			
19.68	$g_{7/2}(f_{7/2})^{-1}$	0.01	0.78	92	0.49
	$g_{9/2}(f_{7/2})^{-1}$	0.06			
21.02	$g_{7/2}(f_{7/2})^{-1}$	0.00	0.13	35	0.05
	$g_{9/2}(f_{7/2})^{-1}$	0.05			

through interference with the GDR, i.e., via a P_1 term in the angular distribution. The very small cross section in the present work prohibited the taking of angular distributions at excitation energies above 21 MeV, but the large P_1 term observed at $E_p = 10$ MeV ($A_1 = 0.22$) is most likely an effect from the low-energy tail of the GQR.

The peak cross section of $7.9 \mu\text{b}$ calculated from LG at the 16.35-MeV peak happens to agree with the experimental value of $7.8 \mu\text{b}$ but the uncertainty in the total width makes it an order-of-magnitude estimate. However, we note on a comparative basis that at higher energies the LG calculation yields smaller peak cross sections than at

16.35 MeV, whereas experimentally, at 19.68 MeV the peak cross section is larger by a factor of 1.4. In fact, the predicted cross section of $0.49 \mu\text{b}$ at that energy is only about 15% of the observed value. In contrast, a similar calculation of the $^{60}\text{Ni}(\gamma, n)$ cross section yields a decrease by a factor of 3 from 16.35 to 19.68 MeV, which is in agreement with the observations of Min and White.²³

Finally, we compare the predictions of LG with the observed angular distributions. If ^{59}Co is again taken as a $1f_{7/2}$ proton hole, the angular distributions can be expressed in general in terms of three normalized partial widths $\Gamma(d_{5/2})$, $\Gamma(g_{9/2})$, $\Gamma(g_{7/2})$ and three relative phases, i.e.,

$$W(\theta) = 1 + \{-0.143\Gamma(d_{5/2}) + 0.476\Gamma(g_{7/2}) - 0.33\Gamma(g_{9/2}) - 0.247[\Gamma(d_{5/2})]^{1/2}[\Gamma(g_{7/2})]^{1/2} \cos[\phi(d_{5/2}) - \phi(g_{7/2})] \\ - 1.464[\Gamma(d_{5/2})]^{1/2}[\Gamma(g_{9/2})]^{1/2} \cos[\phi(d_{5/2}) - \phi(g_{9/2})] - 0.282[\Gamma(g_{7/2})]^{1/2}[\Gamma(g_{9/2})]^{1/2} \cos[\phi(g_{7/2}) - \phi(g_{9/2})]\} P_2(\cos\theta), \quad (4)$$

where $\Gamma(d_{5/2}) + \Gamma(g_{7/2}) + \Gamma(g_{9/2}) = 1$. LG obtained $\Gamma(d_{5/2}) = 0.0$. With allowance made for a sign ambiguity between $[\Gamma(g_{9/2})]^{1/2}$ and $[\Gamma(g_{7/2})]^{1/2}$ and with the ϕ taken as Coulomb phases, the predictions for the 16.35-MeV state are $A_2 = 0.28$ (relative - sign) or $A_2 = 0.03$ (relative + sign). That a positive value is obtained for A_2 regardless of the relative sign, results from the fact that in LG this state is, to a large degree, an $f_{7/2} - g_{7/2}$ excitation. The predicted value obtained for a relative minus sign lies within the range of the experimental value (see Table II). For the 19.68-MeV state, LG predict $A_2 = -0.07$ (relative - sign) or $A_2 = -0.32$ (relative + sign). Again, the value obtained for a relative minus sign is closest to the experimentally observed value.

Thus we find that the GDR calculations of LG are in agreement with the properties observed in the (p, γ) reaction at the lower peak and the neutron data at the higher one, but fail to predict the strong increase of the proton-capture cross section above 17 MeV. On the other hand, this en-

hancement of the proton channel over the largely isospin-forbidden neutron channel is characteristic of the $T_>$ component of the GDR.

B. Calculation with Wave Functions of Good Isospin

We now calculate some properties of the $T_>$ and $T_<$ components of the GDR by building up states of good isospin in a simple 1p-1h model. ^{60}Ni is taken as a closed $f_{7/2}$ proton shell and a closed $p_{3/2}$ neutron subshell, with the same reservations as mentioned previously. The holes are restricted to the $1f_{7/2}$ and $2p_{3/2}$ shells and the particles are allowed into one major shell above the ground state, which leads to the 1p-1h configurations listed in Table V. The target nucleus ^{59}Co is taken as a $1f_{7/2}$ proton hole in a ^{60}Ni core. Radiative capture into the GDR in ^{60}Ni therefore involves proton capture into $2d_{5/2}$, $1g_{9/2}$, and $1g_{7/2}$ orbits.

The coupling of the GDR states to the continuum is calculated using R -matrix theory. Because of the semiquantitative nature of our calculation the well-known problems³⁶ associated with this approach have been ignored. The particle widths are then given by

$$\Gamma_{ij} = 2P_i \gamma_{ij}^2, \quad (5a)$$

where $P_i = \rho/(F_i^2 + G_i^2)$ is the usual penetration factor and γ_{ij}^2 is the reduced width, defined by

$$\gamma_{ij}^2 = (h^2/2MR) C_{ij}^2 u_i^2(R). \quad (5b)$$

C_{ij} is the coefficient, including isospin, of the (l, j) component in the wave function of the GDR. The $u_i(R)$ are the radial wave functions evaluated at the nuclear radius R using harmonic-oscillator wave functions with $h\omega = 41/A^{1/3} \approx 10.5$ MeV. Al-

TABLE V. Configurations which contribute to the GDR in the simple 1p-1h model of the GDR described in the text. The C_{ij}^2 are the products of the 1p-1h expansion coefficients obtained in the schematic model with the appropriate isospin coefficients.

Proton configuration	Neutron configuration	$C_{ij}^2(T_<)$	$C_{ij}^2(T_>)$
	$2d_{5/2}(2p_{3/2})^{-1}$	0.057	
	$3s_{1/2}(2p_{3/2})^{-1}$	0.013	
	$2d_{3/2}(2p_{3/2})^{-1}$	0.006	
$1g_{9/2}(1f_{7/2})^{-1}$	$1g_{9/2}(1f_{7/2})^{-1}$	0.278	0.150
$2d_{5/2}(1f_{7/2})^{-1}$	$2d_{5/2}(1f_{7/2})^{-1}$	0.022	0.012
$1g_{7/2}(1f_{7/2})^{-1}$	$1g_{7/2}(1f_{7/2})^{-1}$	0.008	0.004

though the values of Γ_{ij} so obtained are quite sensitive to the choice of R , ratios of particle widths vary by less than a factor of 2 over the range $6 \leq R \leq 8$ F. In the following, $R = 1.5 \times A^{1/3} = 6$ F is

$$\psi_{>} = \frac{1}{(T_0 + 1)^{1/2}} \sum_i \alpha_i \left[\frac{1}{\sqrt{2}} (|p_i \bar{p}; C\rangle - |n_i \bar{n}; C\rangle) + \sqrt{T_0} |n_i \bar{p}; A\rangle \right] \quad (6)$$

with

$$\sum_i \alpha_i^2 = 1,$$

where p_i, n_i represent protons and neutrons in orbitals above the neutron Fermi level, and \bar{p}, \bar{n} represent holes in orbitals below the proton Fermi level, here restricted to an $f_{7/2}$ hole. C and A are the closed-shell ^{60}Ni core and its analog, respectively. The $T_{<} = T_0$ state consists of three parts, namely, the "anti-analog" configuration to the $T_{>}$ state, the symmetric neutron-proton configuration, and the $T_{<}$ excitations from the neutron excess shell:

$$\psi_{<} = \sum_i \alpha_i \frac{1}{(T_0 + 1)^{1/2}} \left[- \left(\frac{T_0}{2} \right)^{1/2} (|p_i \bar{p}; C\rangle - |n_i \bar{n}; C\rangle) + |n_i \bar{p}; A\rangle \right] + \sum_i b_i \frac{1}{\sqrt{2}} (|p_i \bar{p}; C\rangle + |n_i \bar{n}; C\rangle) + \sum_j c_j |n_j \bar{n}; C\rangle \quad (7)$$

with

$$\sum_i (a_i^2 + b_i^2) + \sum_j c_j^2 = 1.$$

The indices i, j refer again to orbitals above the neutron Fermi level and \bar{n}_x represents a hole in the neutron-excess region, i.e., a $2p_{3/2}$ hole.

The coefficients α_i and a_i, b_i, c_j are now computed in the schematic model for the GDR as outlined by Brown,³⁷ with all 1p-1h energies taken as equal. (This is a rather crude approximation as can be seen from a comparison with the 1p-1h energies used by LG or with experimentally known values.³²⁻³⁴) In this model the coefficients are directly proportional to the dipole absorption matrix elements which have been computed in a square-well potential and are all taken with the same sign. Effective charges $e_p = e(1 - Z/A)$, $e_n = e(-Z/A)$ are used, which are essentially correct for the center-of-mass effect. Since $Z \approx A/2$, the symmetric term in $\psi_{<}$ can be neglected. Also dropped are all 2p-2h matrix elements (i.e., matrix elements involving $|n_i \bar{p}; A\rangle$) but it should be noted that these components make themselves felt through the over-all normalization of the wave function. The resulting coefficients are listed in Table V. In this model the $d_{5/2}$ component does not vanish and the influence of the $g_{7/2}$ component is reduced in comparison with the results of LG, because of the different choice of single-particle energies.

Partial γ widths are easily obtained from the wave functions and lead to a ratio which is written in terms of isospin-reduced and energy-reduced matrix elements

$$\frac{\Gamma_{\gamma(>)} / E_{\gamma^3(>)}}{(1/T_0) \Gamma_{\gamma(<)} / E_{\gamma^3(<)}} = 0.832. \quad (8)$$

used. The prescription given by Goulard, Hughes, and Fallieros⁷ is used to built-up dipole states of good isospin. The state with $T_{>} = T_0 + 1$ has the wave function

Although this ratio is not directly comparable with the experimental data it can be checked against the more general calculation of Fallieros and Goulard.³⁸ Their equivalent formula applied to ^{60}Ni yields a ratio of 0.74, which instills some confidence in our crude model. The larger value obtained for the ratio in our simple calculation can be partially attributed to the weakness of the $E1$ matrix elements associated with the neutron-excess shell in ^{60}Ni ; hence, the relative strengths of the $T_{>}$ and $T_{<}$ components is determined to a larger degree by the isospin factor in Eq. (8). Proton partial widths are obtained from Eqs. (5) and the C_{ij} listed in Table V, with penetrability factors taken for bombarding energies of 7.2 and 10.2 MeV, corresponding to the peak excitation energies of 16.6 and 19.6 MeV, respectively. This procedure yields $\Gamma_{p>} / \Gamma_{p<} = 2.32$. Finally, using the experimentally determined total widths $\Gamma_{<} = 3.4$ MeV and $\Gamma_{>} = 2.7$ MeV, the calculated ratio of peak cross sections turns out to be $\sigma_{>}(p, \gamma_0) / \sigma_{<}(p, \gamma_0) = 1.78$. The experimentally determined ratio taken directly from Fig. 3 is 1.37 while analysis of the data in terms of two Lorentzian curves [Eq. (3)] gives a peak ratio of 1.50. This rather good agreement is simply due to the fact that the cross-section ratio is determined, in essence, by the isospin, energy, and penetration factors.

The wave functions have been generated in too crude an approximation to compute meaningful angular distribution coefficients. However, taking the wave functions at face value, and choosing the sign of $\sqrt{\Gamma_{ij}}$ as the sign of u_{ij} at $R = 6$ F, one obtains $A_2 = +0.24$ at both peaks. This is in poor agreement at the higher peak, although the correct sign is obtained at both. Clearly the $g_{7/2}$

amplitude has been underestimated. We note that the positive sign obtained for A_2 in this case is due to the relative minus sign between the $2d_{5/2}$ and $1g_{9/2}$ wave functions, making the contribution from the $d_{5/2}$ - $g_{9/2}$ interference term in Eq. (4) positive.

Apart from the energies and total widths of the dipole states which may be taken from the data, the model calculation provides all quantities necessary for a rough estimate of the total capture cross section. The absolute normalization of Γ_γ is straightforward. For Γ_p , it must be noted that the penetration factors for a square well have been used above. It has been shown³⁶ that the penetration factor for a more realistic rounded-off potential can be derived from that for a square well by multiplication with an l -independent factor f which in the present case has the value $f \approx 2.5$. On this basis one obtains a proton width $\Gamma_{p_0} \approx 130$ keV and a peak value for the total cross section in the $T_>$ GDR of $\sigma_>(p, \gamma_0) = 7 \mu\text{b}$, which is to be compared with the experimental value of $11 \mu\text{b}$.

One thus finds that in the simple 1p-1h model of the GDR using states of good isospin both the small cross sections and the positive values of A_2 observed in the GDR can be obtained without a major "spin-flip" contribution. The assumption of isospin splitting of the GDR also produces the enhanced (p, γ_0) cross section observed in the region of 19.6-MeV excitation energy. We, therefore, associate the strength observed at 16.6 and 19.6 MeV with the $T_<$ and $T_>$ components of the GDR, respectively.

The possibility that penetrability factors alone might cause the different ratios of proton to neutron yield observed for the two peaks has also been considered. It was assumed that the ratio of proton to neutron reduced widths of the 19.6-MeV state is the same as that of the 16.6-MeV state. By multiplying the observed ratio of proton to neutron yield at 16.6 MeV by the appropriate penetrability factors (evaluated at $R = 6f$), a pre-

dicted ratio at 19.6 MeV is obtained. The factor by which the observed ratio $R(\text{obs})$ exceeds the predicted ratio $R_l(\text{pred})$ for each l value which enters into the simple 1p-1h model is shown in Table VI. It is apparent that the observed ratio of proton yield to neutron yield at 19.6 MeV is from 1.4 to 7 times greater than can be accounted for by penetrability factors alone.

An unanswered question concerns the total widths of the two isospin components of the GDR. If the assignment made above is correct, the width of the $T_>$ state (2.7 MeV) is only slightly smaller than the width of the $T_<$ state (3.4 MeV). This is in contrast to the situation observed in the $A \approx 90$ region, where the $T_>$ component of the GDR generally appears to be fragmented into states with widths of several hundred keV,^{10,11} although the $T_>$ component observed in the reaction $^{88}\text{Sr}(p, \gamma_1)$ - ^{89}Y apparently consists of one dominant resonance ~ 2 MeV wide.¹¹ The possibility that a large neutron width might cause the relatively large total width observed for the $T_>$ component may be considered. The $T_>$ states in ^{60}Ni have in fact, isospin-allowed neutron channels to $T = \frac{5}{2}$ states in ^{59}Ni , as indicated in Fig. 6. An estimate of the relative peak (γ, n) cross sections for the $T_<$ and $T_>$ components, made using the simple 1p-1h model, gives $\sigma_>(\gamma, n)$ as at most a few per cent of $\sigma_<(\gamma, n)$. The (γ, n) data of Min and White²³ are

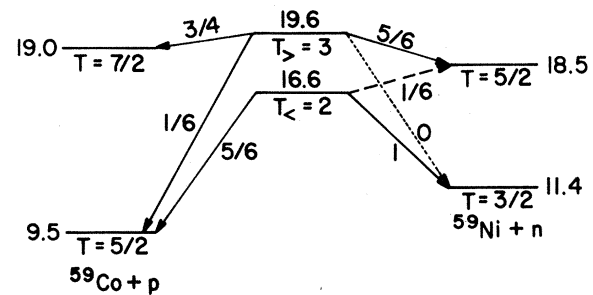


TABLE VI. $R(\text{obs})/R_l(\text{pred})$ gives the factor by which the observed ratio of proton yield to neutron yield at the 19.6-MeV state exceeds the value extrapolated from the 16.6-MeV state by use of appropriate penetrability factors.

Neutron l value	Proton l value	$\frac{R(\text{obs})}{R_l(\text{pred})}$
0	2	6.4
0	4	2.3
2	2	3.7
2	4	1.4
4	2	7.1
4	4	2.7

FIG. 6. Energy levels pertinent to the discussion of the effect of isospin conservation on particle-decay modes of the ^{60}Ni GDR. For the residual nuclei, only the lowest level with the indicated value of isospin is shown. Each solid line indicating an allowed particle-decay mode is labeled with the square of the appropriate isospin-coupling coefficient. The energy-forbidden neutron decay of the $T_<$ 16.6-MeV state to $T = \frac{5}{2}$ levels in ^{59}Ni is indicated by a dashed line, as is the isospin-forbidden neutron decay of the $T_>$ 19.6-MeV state to $T = \frac{3}{2}$ levels in ^{59}Ni . All energies are in MeV and are relative to the ground state of ^{60}Ni .

consistent with $\sigma_{>}(\gamma, n)$ approximately zero to 10% of $\sigma_{<}(\gamma, n)$. Hence, the large total width of the $T_{>}$ GDR cannot be attributed to a large neutron width. A small neutron width also practically eliminates the possibility of a $T_{<}$ contaminant in the $T_{>}$ state, since this would raise the (γ, n) cross section drastically. Indeed, the $T_{>}$ and $T_{<}$ components for the GDR in ^{60}Ni may be quite pure eigenstates of isospin, since their large intrinsic widths might result in lifetimes too short for the Coulomb force to mix the states appreciably. Interference effects between $T_{>}$ and $T_{<}$ states, such as have been clearly observed between analog states and the $T_{<}$ GDR in ^{89}Y ³⁹ and ^{209}Bi ,⁴⁰ have been ignored in the above discussion, since such effects are not apparent in the γ_0 excitation curve.

As outlined in the Introduction, the description of the GDR in terms of states of good isospin yields a definite prediction for the energy splitting between the two components. The averaged effective symmetry energy given by Eq. (2), which gives good results around mass 90, produces a splitting of 3 MeV in ^{60}Ni . Prior to the availability of the proton-capture data, Min²⁶ associated the $T_{<}$ and $T_{>}$ states with strength at 17 and 21.5 MeV, respectively, which results in a 4.5-MeV separation. The value obtained from the present analysis is 3 MeV, in excellent agreement with the prediction.

V. DISCUSSION OF FIRST-EXCITED-STATE TRANSITION

The first excited state in ^{60}Ni at 1.33 MeV, $J^\pi = 2^+$, has, with rather high-purity vibrational character.⁴¹ The GDR based on this state should exhibit structure similar to that observed for the GDR based on the ground state, with the complication that the dipole strength is now distributed among states with the spin values $J^\pi = 1^-, 2^-, 3^-$. The total dipole absorption strength based on the 2^+ state, i.e., the weighted sum for the $1^-, 2^-,$ and 3^- states, should be the same as that from the ground state, and, if the quadrupole surface vibration and the dipole excitation are weakly coupled, the mean strength should be shifted up by about the excitation energy of the 2^+ state, which in the present case is 1.33 MeV. In the opposite case of strong coupling, corresponding peaks should occur in both the γ_1 and γ_0 transitions at the same excitation energy, leading to a more complex structure for the ground-state GDR. The procedure of calculating the energies of the eigenstates depends on the relative periods of the quadrupole surface vibrations and the dipole excitation. A measure of the adiabaticity of the quadrupole and the dipole modes is given by the ratio of characteristic times $\tau(1^-)/\tau(2^+) \cong E_x(2^+)/E_x(\text{GDR}) = 1/13$

for ^{60}Ni . In the case of ^{12}C , where this ratio is 1/5, an extensive calculation by Kamimura, Ikeda, and Arima,⁴² for the ground- and first-excited-state GDR, including strong coupling but not assuming adiabaticity, achieved only moderate success in explaining the data (the question of isospin, of course, does not arise there). The calculation of LG contains strong coupling between the dipole excitation and quadrupole surface modes and assumes adiabaticity, but does not include predictions for the GDR based on the first excited state of ^{60}Ni .

Despite the present lack of a comprehensive theoretical description, we list a few interesting facts indicated by the data. While within the experimental uncertainties corresponding peaks are not present at identical excitation energies in the γ_0 and the γ_1 excitation curves, there is a strong correspondence if the 600-keV averaged γ_1 curve is shifted down in excitation energy by about 300 keV, as noted earlier, except that there are two peaks in the γ_1 curve corresponding to the single 19.6-MeV peak of the γ_0 curve. Angular distributions measured for the γ_1 transition (see Table III) contain large negative A_2 coefficients, in contrast to the angular distributions observed for the γ_0 transition. If angular-distribution coefficients for the γ_1 transition are calculated using the same proton partial widths and relative signs for the $\sqrt{\Gamma_{lj}}$ as those which fit the γ_0 angular distributions [with the simplifying assumptions that $\Gamma(g_{7/2}) = 0$, and that ϕ_{lj} are Coulomb phases], a negative A_2 is obtained only for the dipole state with $J^\pi = 2^-$. In this case $A_2 = -0.165$, which is almost within the experimental limits. For the photonuclear reaction, the entire dipole strength due to the 2^- component of the γ_1 GDR is expected, from a statistical argument, to be $\frac{1}{3}$ of the ground-state strength. As noted above, this is just the integrated cross-section ratio obtained from the data. On the other hand, applying the suggestion made by Segel *et al.*⁴³ in the case of the ^{20}Ne to the present results, the reduced strength observed in the γ_1 GDR might be caused by reduced overlap between 1p-1h GDR states based on the 2^+ excited state in ^{60}Ni and the system $^{59}\text{Co} + p$, as compared with the overlap between 1p-1h GDR states based on the ground state of ^{60}Ni and the $^{59}\text{Co} + p$ system. It is of interest to note, though, that the extensive investigation by Singh *et al.*⁴⁴ of the $^{27}\text{Al}(p, \gamma_1)^{28}\text{Si}$ reaction in the energy region of the γ_1 GDR also led to the conclusion that only the spin assignment 2^- for the γ_1 GDR is compatible with the observed angular distributions. If, however, all the observed dipole strength for the ^{60}Ni γ_1 GDR is attributed to the 2^- component, the problem remains of explaining why the 1^- and 3^- strength should be

missing from the region of excitation energies from 14 to 23 MeV. In the example of ^{12}C , Kami-mura *et al.*⁴² have used theoretical forces which put a substantial part of the 1^- and 3^- strength several MeV above the 2^- excitation. However, this calculation yields an average separation between the γ_0 GDR and the γ_1 GDR which exceeds the excitation energy of the first excited state, which in turn is greater than the experimentally observed separation. In ^{60}Ni a shift of only a fraction of the first-excited-state energy is observed.

Finally, the question concerning the location of the $T_>$ GDR states based on the first excited state remains unanswered. If the structure observed at approximately 20 MeV in the averaged γ_1 excitation function is identified as the $\gamma_1 T_>$ GDR, then the latter would appear to be split, and weaker in comparison to the $T_<$ strength than is the case for the γ_0 GDR. However, it is not apparent why either of these situations should occur.

VI. SUMMARY

The excitation function for the proton-capture reaction leading to the ground state of ^{60}Ni displays two ~ 3 -MeV-wide peaks at 16.6 and 19.6 MeV. These two peaks are interpreted as the $T_< = 2$ and $T_> = 3$ giant dipole resonances, respectively. This is based on a comparison of the inverse (γ, p_0) reaction with the (γ, n) reaction. The latter shows only the lower one of the two peaks whereas the former is enhanced at the higher-energy peak.

Neither a detailed model calculation for the ^{60}Ni 1^- states without consideration of isospin nor penetration-factor considerations alone explain the observations. However, the relative neutron and proton yields at the lower and upper peaks follow the trend expected from isospin-selection rules, and a simple $1p-1h$ model calculation using wave functions of good isospin yields the correct cross-section ratio for the (p, γ_0) reaction at the 16.6- and 19.6-MeV peaks. In the case of ^{60}Ni , the relative strength in the $T_>$ and $T_<$ GDR components is essentially determined by isospin-coupling coefficients. The deduced energy separation $E_{T_>} - E_{T_<} \cong 3$ MeV agrees very well with a general rule which has been successfully applied to the isospin splitting of the GDR around mass 90. The small cross sections and largely isotropic angular distributions can also be explained in the simple model. Structure observed around 22 MeV may be part of the giant quadrupole resonance.

The excitation function for the transition to the 2^+ vibrational first excited state shows a remarkable correspondence to the γ_0 curve if the γ_1 curve is shifted down in excitation energy by ~ 300 keV relative to the γ_0 curve. No quantitative understanding of this cross-section curve exists at this time. Angular distributions and photoproton yield are consistent with the assignment $J^\pi = 2^-$ for most of the 2^+ -based GDR strength up to 21 MeV. The T assignment for the various peaks in the γ_1 curve is not obvious even if taken in analogy to the γ_0 transition.

†Work supported in part by the National Science Foundation.

*A. P. Sloan Foundation Fellow.

‡Permanent address.

¹M. Gell-Mann and V. L. Telegdi, *Phys. Rev.* **91**, 169 (1953).

²H. Morinaga, *Phys. Rev.* **97**, 444 (1955); *Z. Physik* **188**, 182 (1965).

³R. E. Segel, in *Isobaric Spin in Nuclear Physics*, edited by J. D. Fox and D. Robson (Academic Press Inc., New York, 1966).

⁴M. H. MacFarlane, in *Isobaric Spin in Nuclear Physics*, edited by J. D. Fox and D. Robson (Academic Press Inc., New York, 1966).

⁵S. Fallieros, B. Goulard, and R. H. Venter, *Phys. Letters* **19**, 398 (1965).

⁶B. Goulard and S. Fallieros, *Can. J. Phys.* **45**, 3221 (1967).

⁷B. Goulard, T. A. Hughes, and S. Fallieros, *Phys. Rev.* **176**, 1345 (1968).

⁸T. A. Hughes and S. Fallieros, in *Nuclear Isospin*, edited by J. D. Anderson, S. D. Bloom, J. Cerny, and W. W. True (Academic Press Inc., New York, 1969).

⁹S. Fallieros, private communication.

¹⁰M. Hasinoff, G. A. Fisher, H. M. Kaun, and S. S. Hanna, *Phys. Letters* **30B**, 337 (1969).

¹¹J. F. Amann, N. Cue, E. M. Diener, and P. Paul, *Bull. Am. Phys. Soc.* **15**, 455 (1970).

¹²E. M. Diener, P. Paul, and J. F. Amann, *Bull. Am. Phys. Soc.* **15**, 593 (1970).

¹³R. E. Segel, L. Meyer-Schützmeister, D. S. Gemmell, R. C. Bearse, N. G. Puttaswamy, H. J. Fortune, J. V. Maher, and E. L. Sprenkel-Segel, *Bull. Am. Phys. Soc.* **15**, 47 (1970).

¹⁴S. Fallieros, *Bull. Am. Phys. Soc.* **15**, 624 (1970).

¹⁵N. V. Lin'Kova, R. M. Osokina, B. S. Ratner, R. Sh. Amirov, and V. V. Akindinov, *Zh. Eksperim. i Teor. Fiz.* **38**, 780 (1959) [transl.: *Soviet Phys.-JETP* **11**, 566 (1960)].

¹⁶D. McPherson, E. Pederson, and L. Katz, *Can. J. Phys.* **32**, 593 (1954).

¹⁷L. Katz, R. N. H. Haslam, J. Goldemberg, and J. G. V. Taylor, *Can. J. Phys.* **32**, 580 (1954).

¹⁸B. S. Ishkhanov, E. N. Kornienko, Yu. I. Sorokin, V. G. Shevchenko, and B. A. Yur'ev, *Zh. Eksperim. i Teor. Fiz.* **45**, 38 (1963) [transl.: *Soviet Phys.-JETP* **18**, 29 (1964)].

¹⁹I. I. Dushkov, B. S. Ishkhanov, I. M. Kapitnov, B. A.

- Yur'ev, and V. G. Shevchenko, Phys. Letters 10, 310 (1964).
- ²⁰T. K. Deague, E. G. Muirhead, and B. M. Spicer, Nucl. Phys. A139, 501 (1969).
- ²¹T. D. Urbas and J. J. Stewart, Phys. Letters 24, 1026 (1970).
- ²²See, for example, J. J. Stewart, H. J. Weber, and J. J. Stewart, Phys. Rev. 182, 1359 (1969).
- ²³K. Min and W. Greiner, Phys. Rev. 182, 1200 (1968).
- ²⁴B. I. Goryachev, B. I. Goryachev, I. M. Kapitnov, I. M. Piskarev, V. G. Shevchenko, and O. P. Shevchenko, ZhETF Pis'ma v Redaktsiyu 8, 76 (1968) [transl.: JETP Lett. 8, 46 (1968)].
- ²⁵D. G. Owen, E. G. Muirhead, and B. M. Spicer, Nucl. Phys. A140, 523 (1970).
- ²⁶K. Min, Phys. Rev. 182, 1359 (1969).
- ²⁷E. M. Diener, J. F. Amann, S. L. Blatt, and P. Paul, Nucl. Instr. Methods 83, 115 (1970).
- ²⁸F. S. Dietrich, M. Suffert, A. V. Nero, and S. S. Hanna, Phys. Rev. 168, 1169 (1968).
- ²⁹E. M. Diener, P. Paul, S. L. Blatt, J. F. Amann, and L. L. Lee, Bull. Am. Phys. Soc. 14, 584 (1969).
- ³⁰M. Danos and W. Greiner, Phys. Rev. 138, B876 (1965).
- ³¹R. Ligensa and W. Greiner, Ann. Phys. (N.Y.) 51, 28 (1969).
- ³²B. L. Cohen, R. H. Fullmer, and A. L. McCarthy, Phys. Rev. 126, 698 (1962).
- ³³A. G. Blair, in Argonne National Laboratory Report No. ANL-6878, 1964 (unpublished), p. 128.
- ³⁴R. H. Follmer, A. L. McCarthy, and B. L. Cohen, Phys. Rev. 133, B955 (1964).
- ³⁵R. J. J. Stewart, J. C. Morrison, and D. E. Frederick, Phys. Rev. Letters 23, 323 (1969).
- ³⁶G. Michaud, L. Scherk, and E. Vogt, Phys. Rev. C 1, 864 (1970).
- ³⁷G. E. Brown, *Unified Theory of Nuclear Models and Forces* (North-Holland Publishing Co., Amsterdam, The Netherlands, 1967).
- ³⁸S. Fallieros and B. Goulard, Nucl. Phys. A147, 593 (1970).
- ³⁹N. Cue, J. F. Amann, P. Paul, and E. M. Diener, Bull. Am. Phys. Soc. 14, 1238 (1969).
- ⁴⁰K. A. Snover, J. F. Amann, W. Hering, and P. Paul, to be published.
- ⁴¹D. Cline, H. S. Gertzman, H. E. Gove, P. M. S. Lesser, and J. J. Schwartz, Nucl. Phys. A133, 445 (1969).
- ⁴²M. Kamimura, K. Ikeda, and A. Arima, Nucl. Phys. A95, 129 (1968).
- ⁴³R. E. Segel, Z. Vager, L. Meyer-Schützmeister, P. P. Singh, and R. G. Allas, Nucl. Phys. A93, 31 (1967).
- ⁴⁴P. P. Singh, R. E. Segel, L. Meyer-Schützmeister, S. S. Hanna, and R. G. Allas, Nucl. Phys. 65, 577 (1965).

Reaction $^{36}\text{Ar}(d, p)^{37}\text{Ar}^\dagger$

S. Sen, C. L. Hollas, and P. J. Riley

Center for Nuclear Studies, The University of Texas, Austin, Texas 78712

(Received 1 February 1971)

The level structure of ^{37}Ar has been investigated via the reaction $^{36}\text{Ar}(d, p)^{37}\text{Ar}$ at an incident deuteron energy of 9.162 MeV and with an over-all energy resolution of approximately 30 keV. A total of 53 states of ^{37}Ar with excitation energies up to 9.012 MeV have been observed. The orbital-angular-momentum-transfer values and the spectroscopic factors for 29 of the observed states have been extracted using finite-range distorted-wave Born-approximation calculations corrected for nonlocality of the optical potential. One $l=0$, two $l=2$, three $l=3$, and twenty-three $l=1$ transfer values have been assigned. Spin assignments have been made on the basis of the conventional shell-model ordering of states, by comparison of the states of ^{37}Ar with those of the mirror nucleus ^{37}K , and on the basis of the Lee-Schiff effect. The spin, parity, excitation energies, and the spectroscopic factors obtained for the lowest few states in ^{37}Ar are in fair agreement with those predicted through recent shell-model calculations.

I. INTRODUCTION

The deuteron stripping reaction has proved to be an extremely useful tool for obtaining nuclear spectroscopic information, because of the unique dependence of the shape of the (d, p) angular distribution on the orbital-angular-momentum transfer.¹ The energy levels of the ^{37}Ar nucleus via the reaction $^{36}\text{Ar}(d, p)^{37}\text{Ar}$ have not been extensively investigated.²⁻⁵ Rosner and Schneid⁴ studied this reaction with an ^{36}Ar gas target enriched to >99%,

using a cyclotron and solid-state detectors. The limited energy resolution (of the order of 80 keV) allowed spin assignments to be made for only seven relatively strongly excited states. Holbrow *et al.*⁵ studied the same reaction using a tandem accelerator in conjunction with a magnetic spectrograph and obtained an energy resolution of approximately 20 keV. They observed a total of 76 excited states of ^{37}Ar , but since angular-distribution measurements were not carried out, spin and parity assignments were not made. The present